



Bayesian inverse modeling and source location of an unintended I-131 release in Europe in the fall of 2011

Ondřej Tichý¹, Václav Šmídl¹, Radek Hofman¹, Kateřina Šindelářová¹, Miroslav Hýža², and Andreas Stohl³

¹Institute of Information Theory and Automation, Czech Academy of Sciences, Prague, Czech Republic

²National Radiation Protection Institute, Prague, Czech Republic

³NILU: Norwegian Institute for Air Research, Kjeller, Norway

Correspondence to: Ondřej Tichý (otichy@utia.cas.cz)

Abstract. In the fall of 2011, iodine-131 (I-131) was detected at several radionuclide monitoring stations in Central Europe. After investigation, the International Atomic Energy Agency (IAEA) was informed by Hungarian authorities that I-131 was released from the Institute of Isotopes Ltd in Budapest, Hungary. It was reported that a total activity of 342 GBq of I-131 was emitted between September 8 and November 16, 2011. In this study, we use the ambient concentration measurements
5 of I-131 to determine the location of the release as well as its magnitude and temporal variation. Although the location of the release became eventually known, its temporal variation is still uncertain and only partial information is available. For our source reconstruction, we use no prior knowledge. Instead, we estimate the source location and emission variation using only the available I-131 measurements. Subsequently, we use the information about the source term for validation of our results. For the source determination, we first perform backward runs of atmospheric transport models and obtain source-
10 receptor-sensitivity (SRS) matrices for each grid cell of our study domain. We use two dispersion models, Flexpart and Hysplit, driven with meteorological analysis data from the global forecast system (GFS) weather forecast model. Second, we use a recently developed inverse method, least-squares with adaptive prior covariance (LS-APC), to determine the I-131 emissions and their temporal variation from the measurements and computed SRS matrices. For each grid cell of our simulation domain, we evaluate the probability that the release was generated in that cell using Bayesian model selection. The model selection
15 procedure also provides information about the most suitable dispersion model for the source term reconstruction. Third, we select the most probable location of the release with its associated source term and perform forward calculation to study the consequences of the iodine release. Results of these procedures are compared with the known release location and reported information about its time variation. We find that our algorithm could successfully locate the actual release site. The estimated release period is also in agreement with the values reported by IAEA, while our estimate for the total released activity (490
20 GBq) is higher than the reported one (342 GBq). Nevertheless, even using our larger source term, dose amounts were very low and never exceeded regulatory limits.



1 Introduction

In the fall of 2011, I-131 was detected in the atmosphere by the European Trace Survey Stations Network for Monitoring Airborne Radioactivity (Ring of 5, Ro5). The measured values were very low, up to a few tens of $\mu\text{Bq m}^{-3}$, close to the minimum detectable activity of the instruments. After the first findings in Austria and their subsequent confirmation by Czech laboratories, it was clear that these detections could not be explained by local sources. Hence, the International Atomic Energy Agency (IAEA) was informed on November 11 and launched an investigation. Detectable concentrations of I-131 were afterwards also measured by other laboratories, mainly in Central Europe (Atomic Energy Agency, 2011a). Based on the information provided by other Ro5 laboratories and a rough assessment of meteorological conditions, it was estimated that the source was likely located east of Austria and the Czech Republic. This was later confirmed when the IAEA Incident and Emergency Centre (IEC) was informed by the Hungarian Atomic Energy Authority (HAEA) (Atomic Energy Agency, 2011b) that I-131 was released from the Institute of Isotopes (IoI) Ltd, Budapest, a facility that produces I-131 mainly for healthcare such as thyroid diagnosis. It is thought that a failure in the dry distillation process caused the emissions (Gitzinger et al., 2012). It was later reported that between September 8 and November 16, 2011, a total activity of 342 GBq of I-131 was released from the institute, with a maximum release intensity of 108 GBq between October 12 and October 14. The release is thought to have occurred through the 80 meters high stack of the institute. Since the released activity was below the institute's authorized annual radioactive release limit and I-131 concentrations in the air were very low, IAEA stated that the situation did not pose a health risk.

Although some ambient concentration measurements are available for this case, they are quite sparse, poorly resolved in time (typically sums over 7 days), and cover many orders of magnitude. This makes an analysis of the impact of the event based on measurement data alone very difficult. For example, if no measurements are available in the area of the largest impact, the severity of the event may be grossly underestimated. Given accurate release information, atmospheric transport models can simulate the radioiodine dispersion and give a more comprehensive view of the situation than the measurements alone. For instance, simulations with atmospheric transport models were used previously to study the distribution of radioactive material after the Chernobyl (Brandt et al., 2002; Davoine and Bocquet, 2007) and Fukushima Dai-ichi nuclear accidents (Morino et al., 2011; Stohl et al., 2012; Saunier et al., 2013). Simulations were also already made for the I-131 release from IoI in 2011 (Leelőssy et al., 2017). However, the agreement between the results of simulations and real measurements needs to be carefully evaluated since simulations often suffer from inaccuracies in meteorological input data or model parametrizations. The largest errors in such simulations are arguably caused by uncertainties in the source term of the release, i.e., the rate of emissions into the atmosphere as a function of time. However, the release term is often not known and its determination can be particularly difficult in case of a nuclear accident since the release can last for a long time and its intensity can vary by orders of magnitude.

To our best knowledge, the exact source term in the case of the Hungary iodine release in 2011 is unknown and only approximate and vague information is available (Gitzinger et al., 2012). For lack of information on the operating conditions of the isotope production facility, we cannot use the so-called bottom-up approach where the source term is quantified based on understanding and modeling of the emission process. Therefore, in this paper we use the so-called top-down approach (Nisbet and Weiss, 2010), which combines ambient concentration measurements with an atmospheric transport model and an



optimization algorithm to determine the source term. This approach is also called inverse modeling. The source term is typically estimated as a result of optimization of the difference between the measurements and corresponding simulated sensor readings predicted by the atmospheric transport model. Due to insufficient information provided by the measurement data, the problem has to be regularized using a penalty function (Seibert, 2000; Eckhardt et al., 2008), the maximum entropy principle (Bocquet, 2005), or a variational Bayesian approach (Tichý et al., 2016). All these methods assume that the measurement vector can be described as a linear model with a source-receptor-sensitivity (SRS) matrix (calculated using an atmospheric dispersion model, Seibert and Frank (2004)) and unknown source term vector.

The range of possible regularizations techniques starts with simple Tikhonov penalty (Davoine and Bocquet, 2007) and additional enforcement of temporal and/or spatial smoothness of the release (Eckhardt et al., 2008). Interpretation of the regularization as a prior covariance matrix allows its estimation. Different methods exist for parametrizations of both the measurements covariance matrix and source term covariance matrix. Winiarek et al. (2012) parameterize each covariance matrix using one common parameter on its diagonal. A similar model was also studied by Michalak et al. (2005) with different diagonal entries and by Berchet et al. (2013) with full unknown covariance matrices, however, with convergence issues since too many parameters need to be estimated in this case. Therefore, non-diagonal matrix elements are often parametrized using autocorrelation parameters that link covariance in space and/or time (Ganesan et al., 2014; Henne et al., 2016). In this paper, we follow a previously developed approach (Tichý et al., 2016) where the source term covariance matrix is adaptively estimated within the estimating procedure using a variational Bayes methodology (Šmídl and Quinn, 2006).

An application of the inverse modeling problem is the source location problem. If the release site is unknown, the inverse modeling is performed for many potential release sites and their likelihood of being the correct site is compared. The simplest scenarios assume a constant release rate (Annunzio et al., 2012; Zheng and Chen, 2010; Ristic et al., 2016) or even steady wind field (Liping et al., 2013). However, these are not very realistic assumptions, especially not for complex emission scenarios with continental-scale impacts.

Typically, the inverse modeling problem is recast as an optimization problem such as the weighted linear or nonlinear least squares (Singh and Rani, 2014; Matthes et al., 2005), simulated annealing (Thomson et al., 2007), or pattern search method (Zheng and Chen, 2010). Cervone and Franzese (2010) studied several error functions to identify suitable measures and cost functions for optimizations and Kovalets et al. (2011) used a fluid dynamics model to build up a cost function which could be optimized. These methods can be inconvenient due to problematic convergence and limited information on the uncertainty of the results. Often, they provide only point estimates. Full posterior probability densities are provided using Bayesian techniques where the prior model is typically constructed as an alternative to the cost function in the optimization approach. Very popular Bayesian inference techniques are random search algorithms such as Markov chain Monte Carlo (MCMC) methods. Examples for this type of approach are Keats et al. (2007), Senocak et al. (2008) where also wind field parameters are estimated along with the source term parameters, or Delle Monache et al. (2008) who studied the Algeciras accidental release with the assumptions that the source geometry and release time are known. Another Bayesian formulation and inference using maximum entropy principle was proposed by Bocquet (2007) where the source term is modeled as three-dimensional (area plus time); hence, the source term integrated over time and area is obtained. This approach was tested for both cases of the European tracer



experiment (ETEX) (Krysta et al., 2008) and compared with the maximum posterior estimator by Bocquet (2008) with further non-Gaussian assumptions such as positivity or boundedness. Recently, a likelihood-free approximate Bayesian computation method for the localization of a biochemical source was proposed by Ristic et al. (2015) where multiple dispersion models can be used and even weighted using Bayesian model selection. Our team has developed a Bayesian inverse method (Tichý et al., 2016) called least-squares method with adaptive prior covariance (LS-APC) based on a flexible covariance matrix of the source term. The model was validated on the basis of the ETEX experiment and it was shown that the dependency on manual selection of model parameters is lower than in case of its predecessors.

In this paper, we use the LS-APC method for inversion for the case of the iodine release in Hungary in 2011. Moreover, we derive the Bayesian model selection for the LS-APC model. Using this methodology, we can compare the reliability of each SRS matrix from the selected spatial domain. The SRS matrices are computed using backward runs of the dispersion models Flexpart (Stohl et al., 2005) and Hysplit (Draxler and Hess, 1997) which were based on meteorological input data from GFS meteorological fields with resolution of $0.5^\circ \times 0.5^\circ$ in the case of Flexpart and with resolutions $0.5^\circ \times 0.5^\circ$ and $1^\circ \times 1^\circ$ in the case of Hysplit. We identify the most probable release location and derive the corresponding estimated source term. Using this source information, we perform a forward run and produce a I-131 dose map for Europe that can be used for impact assessment.

2 Measurement data

Iodine can exist in the atmosphere both as a gas and in the aerosol phase. Measurements of particulate phase I-131 were made at several stations of the Ro5 network, which is an informal information group established in 1983 for the purpose of rapidly exchanging data on occasional enhanced concentrations of man-made radionuclides at trace levels. In total, 117 I-131 measurements from 11 different sampling sites in Central Europe (see details in Table 1) obtained from September to November 2011 were used in this study.

Atmospheric aerosol sampling was performed using various types of high volume samplers with flow rates ranging from 150 to 900 m³/h. In these devices, the air is filtered through glass-fiber or polypropylene filters which capture the radioactive aerosol with a high efficiency. As the laboratories operate under their own monitoring plans, sampling intervals differ both in length and starting day. In general, filters are changed every 3–7 days under normal conditions. Only in case of an emergency situation, the sampling period would be shortened.

After the sampling completion and decay of short-lived radon decay products, the filters are measured without additional chemical preparation in laboratories equipped with a high resolution gamma ray spectrometer. Since I-131 emits 364 keV photons with an intensity of 81%, it allows a reasonably sensitive determination by a high-purity germanium (HPGe) spectrometer. In such a measurement arrangement, it is possible to achieve detection limits of several $\mu\text{Bq}/\text{m}^3$ but at the cost of a rather poor time resolution. Considering the 8.02 day half-life of I-131, the resulting activity value has to be decay corrected which requires the assumption that the concentration in the air was constant during sampling.



3 Inverse modeling

We follow the concept of linear modeling of the atmospheric dispersion using a source-receptor sensitivity (SRS) matrix (Wotawa et al., 2003). In this approach, an atmospheric transport model is used to provide the linear relationship between sources and atmospheric concentrations. By assuming a release x_i from the release site at time i , we can calculate the concentration response at a receptor y_j at time j . Notice that the simulated concentration response can be compared directly with measured concentrations at the receptor. The ratio $m_{ij} = y_j/x_i$ defines the source receptor sensitivity. Collecting all possible release times in vector $\mathbf{x} \in \mathbf{R}^n$ and all possible receptor responses at all measurement sites and times into vector $\mathbf{y} \in \mathbf{R}^p$ we obtain a linear model

$$\mathbf{y} = M\mathbf{x} + \epsilon, \quad (1)$$

where $M \in \mathbf{R}^{p \times n}$ is a SRS matrix and $\epsilon \in \mathbf{R}^p$ is an overall observation error including both model and measurement errors, where the model error contained in matrix M is projected onto the observation vector. This concept of SRS is quite universal and can be applied with both Lagrangian and Eulerian transport models in both forward and backward runs (Seibert and Frank, 2004). However, the assumption of linearity is justified only for passive tracers and substances which do not undergo nonlinear chemical transformations – which is largely the case for iodine, which is thought to have mainly linear removal processes (radioactive decay and wet and dry deposition to the surface).

An estimate of the unknown vector \mathbf{x} can be obtained using minimization of the model error (1). However, a Bayesian approach provides more informative results since it evaluates the full posterior density of the unknown. The high computational cost of conventional Monte Carlo evaluation methods can be avoided by using an approximation technique known as Variational Bayes. This has been analyzed in detail by Tichý et al. (2016), where a computationally efficient algorithm was presented. One of the key advantages is that all parameters of the regularization are estimated together with the source term. In this paper, we provide an approximate formula for the evaluation of the marginal likelihood of the model, which is essential for Bayesian model comparison (Bernardo and Smith, 2009). In effect, this technique allows to compare the likelihood of different matrices M which could describe atmospheric dispersion from different possible source locations or could originate from different atmospheric dispersion models.

Before reviewing the full probabilistic model, we would like to illustrate its relation to the conventional cost optimization. Consider the quadratic norm of the residues of (1)

$$J = \omega_0^{-2} (M\mathbf{x} - \mathbf{y})^T (M\mathbf{x} - \mathbf{y}), \quad (2)$$

with selected parameter ω_0 . The estimate $\langle \mathbf{x} \rangle$ can be obtained by minimizing the cost J (Eq. 2) plus additional regularization terms. In probabilistic interpretation, minimization of Eq. 2 is equivalent to maximization of the likelihood function

$$p(\mathbf{y}|\mathbf{x}) = \mathcal{N}(M\mathbf{x}, \omega_0^{-1}I_p) \propto \exp\left(-\frac{1}{2}\omega_0(M\mathbf{x} - \mathbf{y})^T(M\mathbf{x} - \mathbf{y})\right), \quad (3)$$

where $\mathcal{N}(\boldsymbol{\mu}, \Sigma)$ denotes a multivariate Gaussian distribution with mean $\boldsymbol{\mu}$ and covariance matrix Σ , I_p is the $p \times p$ identity matrix, and symbol \propto denotes equality up to the normalizing constant. In this case, $\Sigma = \omega_0^{-1}I_p$ and ω_0 is known as the precision



parameter. The normalization constant is irrelevant for maximization. However, it will become important for estimating the precision parameter ω_0 . Due to the requirement of normalization, the Bayesian method allows to estimate parameters of the prior distributions (which define the regularization terms in the cost formulation). To distinguish between selected and estimated parameters, we denote all preselected parameters with subscript 0 and estimated model parameters without the subscript.

5 After reviewing the selected Bayesian inverse method, we will study the model selection property for the model in Sect. 3.2.

3.1 Review of Bayesian inverse method LS-APC

The probabilistic model of Tichý et al. (2016) is briefly reviewed in this Section. The likelihood function is considered to be Gaussian (3) with standard deviation ω being considered as unknown. Thus, we need to select its prior distribution. We select the gamma distribution due to its conjugacy with Gaussian likelihood (Tipping and Bishop, 1999):

$$10 \quad p(\mathbf{y}|\mathbf{x}, \omega) = \mathcal{N}(M\mathbf{x}, \omega^{-1}I_p), \quad (4)$$

$$p(\omega) = \mathcal{G}(\vartheta_0, \rho_0), \quad (5)$$

where ϑ_0, ρ_0 are chosen constants. These constants are needed for numerical stability, however, they are set as low as possible to provide a non-informative prior.

The prior distribution of the source term \mathbf{x} is designed to encourage three properties: i) non-negativeness of all elements of \mathbf{x} , ii) sparsity, i.e., the element is zero unless there is sufficient information on the opposite, and iii) smoothness, i.e. that rapid changes in the temporal profile are possible but not frequent. These properties are encoded into a hierarchical prior model

$$p(x_{j+1}|x_j, l_j, v_j) = t\mathcal{N}(-l_j x_j, v_{j+1}^{-1}, [0, \infty]), \quad \text{for } j = 1, \dots, n-1, \quad (6)$$

$$p(v_j) = \mathcal{G}(\alpha_0, \beta_0), \quad \text{for } j = 1, \dots, n, \quad (7)$$

$$p(l_j|\psi_j) = \mathcal{N}(-1, \psi_j^{-1}), \quad \text{for } j = 1, \dots, n-1, \quad (8)$$

$$20 \quad p(\psi_j) = \mathcal{G}(\zeta_0, \eta_0), \quad \text{for } j = 1, \dots, n-1, \quad (9)$$

where $t\mathcal{N}(\mu, \sigma, [a, b])$ denotes the truncated Gaussian distribution on support $[a, b]$, l_j is a parameter modeling the smoothness, i.e. the relation between neighboring elements of the source term, and v_j is its precision parameter. The prior for element x_1 is $p(x_1|v_1) = \mathcal{N}(0, v_1^{-1}, [0, \infty])$. The prior has constants $\alpha_0, \beta_0, \zeta_0, \eta_0$ that need to be selected. Good performance was reported with their non-informative choice, e.g., 10^{-10} . The estimation algorithm for this model using the variational Bayes methodology (Šmídl and Quinn, 2006) is available in Matlab code as a supplement of Tichý et al. (2016).

3.2 Bayesian model selection

In a situation where multiple SRS matrices are available it is possible to consider a task of selecting the most likely matrix for the observed data. This situation arises in the source location problem, where one SRS is generated for each potential release site, for selection between different atmospheric dispersion models (or the same model driven with different meteorological input data), or when varying uncertain parameters in a dispersion model. Formally, we define a finite set of SRS matrices,



$\mathcal{M} = \{M_1, \dots, M_r\}$ and consider the task of estimating the probability of each matrix jointly with all parameters of model (4)–(9). This can be achieved by extension of the Variational Bayes methodology (Bishop, 2006) where the probability $p(M_i)$ for each SRS matrix is computed as

$$p(M_i) \propto p_0(M_i) \exp(\mathcal{L}_{M_i}), \quad (10)$$

- 5 where $p_0(M_i)$ is a prior probability for M_i which can be set to $p_0(M_i) = 1/r$ for each i when no prior assumption is made (as in our case) and \mathcal{L}_{M_i} is a variational lower bound on $p(\mathbf{y})$ given as

$$\mathcal{L}_{M_i} = \int p(\mathbf{x}, \Upsilon, L, \psi, \omega | M_i) p(M_i) \ln \frac{p(\mathbf{y}, \mathbf{x}, \Upsilon, L, \psi, \omega, M_i)}{p(\mathbf{x}, \Upsilon, L, \psi, \omega | M_i) p(M_i)} d\mathbf{x} d\Upsilon dL d\psi d\omega. \quad (11)$$

Eq. (11) can be seen as a term composed of expected values (denoted as $E[\cdot]$ with respect to distribution of the variable in its argument) so that

10

$$\mathcal{L}_{M_i} = E[\ln p(\mathbf{y}, \mathbf{x}, \Upsilon, L, \psi, \omega, M_i)] - E[\ln \tilde{p}(\omega)] - E[\ln \tilde{p}(\mathbf{x})] - E[\ln \tilde{p}(\Upsilon)] - E[\ln \tilde{p}(L)] - E[\ln \tilde{p}(\psi)], \quad (12)$$

where $p(\mathbf{y}, \mathbf{x}, \Upsilon, L, \psi, \omega, M_i)$ is the joint distribution of likelihood (4) and prior probability distributions (6)–(9), and $\tilde{p}(\cdot)$ are posterior probability distributions. These terms are given in the supplementary material.

4 Atmospheric transport modeling

- 15 The SRS matrices in this work were computed using backward runs of two alternative models, namely Hysplit (Draxler and Hess, 1997) and Flexpart (Stohl et al., 2005). As the domain of interest we chose the region spanning from 5° E to 30° E in longitude and from 40° N to 65° N in latitude covering most of Europe and parts of the Mediterranean Sea. Horizontally, the domain was discretized into 2500 grid cells with resolution $0.5^\circ \times 0.5^\circ$ which approximately corresponds to 45 km \times 55 km at the latitude of Budapest. Vertically, there is no discretization of the domain and sensitivities are calculated for a layer 0-300 m
20 above ground which allows for both ground and somewhat elevated releases (e.g., through the stack of the isotope production facility). Mixing heights are often higher than 300 m, in which case the result is not very sensitive to the choice of the depth of this layer. Temporal resolution of the source was set to 1 day and we assume that the release occurred during a 91 day time window starting on 1 September 2011.

- As a result, the domain was discretized into 227500 spatio-temporal sources for which their possible contributions to all
25 samples must be calculated. Since the number of candidate sources is much higher than the number of measurement samples, the SRS matrices were obtained using backward runs of the model from the sampling sites. One backward run was started exactly at the point location of each measurement site and for each period corresponding exactly to a measurement sample. Each of the 117 backward runs corresponding to the 117 available measurements provided a SRS matrix of a particular sample to all candidate spatio-temporal sources in our domain. Since we a-priori assume that the release occurred from a point source
30 (i.e., a single horizontal grid cell), we can calculate SRS fields from a single grid cell at once which allows parallelization of the computations. We end up with 2500 SRS matrices of dimension 117×91 from each transport model.



Radioiodine can be present in the atmosphere as molecular I_2 , as organic iodide, or as iodide salts. The former two are expected to exist as gases, while the latter is an aerosol. In which form iodine is released to the environment from a nuclear facility depends on its operating conditions (Simondi-Teisseire et al., 2013). Iodine chemistry in the atmosphere is complex and can involve, for instance, chemical transformation of the different compounds and particle formation (Saiz-Lopez et al., 2012). As every compound has its own scavenging efficiency, both with respect to dry and wet deposition, accurate modeling of iodine is complicated. We chose a simple approach for our modeling, namely assuming that all released I-131 was in particulate form, which most probably dominated the release. This is also justified by the fact that all of the measurements we have available were made for particulate iodine only. Consequently, in both models, I-131 was simulated as an aerosol. In Flexpart, parameters of the dry and wet deposition were set to default values for I-131 in the Flexpart 9.2 species library and radioactive decay (ingrowth during backward runs) was calculated on the fly. In Hysplit, parameters of the dry and wet deposition were set to default values for aerosol I-131, except for predefined dry deposition velocity which was set to 5.7 mms^{-1} according to measurements of Takeyasu and Sumiya (2014). Hysplit calculated with I-131 radioactive decay half-life of 8 days. Our inverse modeling would thus not capture gaseous I-131, which may have been co-emitted, except indirectly if some of this gaseous I-131 condensed on or formed particles that were subsequently measured. Our results are thus lower estimates of the total I-131 release, but the bias is probably not very large.

4.1 Flexpart

Flexpart (FLEXible PARTicle dispersion model) is a scientific model used worldwide by many research groups and also operationally, e.g. at CTBTO for routine atmospheric backtracking (Kalinowski et al., 2008). In this work we used version 9.2 (Stohl et al., 2005). Runs were forced with GFS meteorological fields with $0.5^\circ \times 0.5^\circ$ horizontal resolution and 26 vertical layers and temporal resolution of 3 hours. During all calculations, the convection scheme was enabled in Flexpart for more realistic simulation of vertical air mass fluxes when convective conditions are encountered (Forster et al., 2007).

Simulations in Flexpart can be carried out on two different output grids in a single run. The so called mother grid is usually a global grid with coarser resolution whereas the nested grid is a smaller subdomain with higher horizontal resolution (vertical resolution must be the same for both grids). Our domain of interest was a nested output grid with horizontal resolution $0.5^\circ \times 0.5^\circ$ whereas the global grid with resolution $1^\circ \times 1^\circ$ was the mother grid. The simulations accounted for dry deposition using a resistance method. Wet scavenging was accounted for with a scheme that distinguishes between in-cloud and below-cloud scavenging.

4.2 Hysplit

The Hysplit (HYbrid Single-Particle Lagrangian Integrated Trajectory) model was used as an alternative to Flexpart simulations. Hysplit is a model widely used to simulate atmospheric transport and dispersion on various levels of complexity. Its applications range from simple estimation of forward and backward trajectories of air parcels, to advanced modeling of transport, dispersion and deposition of air masses on large domains. Hysplit adopts a hybrid approach combining the Lagrangian (moving frame of reference for diffusion and advection) and Eulerian (fixed model grid for calculation of air concentration)



model methodologies. In this study we applied Hysplit model version 4 (Draxler and Hess, 1997, 1998; Draxler and Rolph, 2003; Stein et al., 2015).

The model was forced with GFS analyses with horizontal resolution of $0.5^\circ \times 0.5^\circ$, 26 vertical layers and 3-hourly temporal resolution. The model domain covered most of the European continent. The Hysplit model was also forced with GFS analyses with horizontal resolution of $1^\circ \times 1^\circ$, 26 vertical layers and 6-hourly temporal resolution, to test the sensitivity of the source re-construction to meteorological input data resolution. This data set was only available in a format suitable for Hysplit but not for Flexpart. The resolution of the output grid was the same as used with Flexpart, i.e., $0.5^\circ \times 0.5^\circ$.

5 Results and discussion

In this Section, we apply the Bayesian inverse modeling method introduced in Sect. 3 to iodine measurements described in Sect. 2 and computed SRS matrices from Sect. 4 for all three cases: (i) Flexpart driven with the GFS analyses with the resolution $0.5^\circ \times 0.5^\circ$ (Flexpart-GFS-0.5), (ii) Hysplit driven with the GFS analyses with the resolution $0.5^\circ \times 0.5^\circ$ (Hysplit-GFS-0.5), and (iii) Hysplit driven with the GFS analyses with the resolution $1^\circ \times 1^\circ$ (Hysplit-GFS-1.0). First, we will study the problem of source location, and after that we will discuss the source term as a function of time for the most probable source location.

5.1 Source location

The LS-APC inversion method was applied to each grid cell in our domain as described in Sect. 3. The method also provides the variational lower bound \mathcal{L}_{M_i} , Eq. (12). The results are presented in Fig. 1 for Flexpart-GFS-0.5 (left), Hysplit-GFS-0.5 (middle), and Hysplit-GFS-1.0 (right).

In all three cases, the source location mechanism of the LS-APC method works very well and the maxima of the variational lower bound \mathcal{L}_{M_i} are close to the true location of the IoI. Note that the exact location of the IoI is 18.96° E 47.49° N which is in the corner of discretization in the case of 0.5° resolution; hence, we assume all results close to this point to be very good. In the case of Flexpart-GFS-0.5, actual release site is on the edge of the estimated release grid cell, while for both Hysplit cases, the actual release site is one grid cell away from the estimated release grid cell. In all three cases, some uncertainty remains especially to the south of the IoI where no measured data are available while in the north, the uncertainty is very small because the relatively dense measurement network there effectively excludes the possibility of a source in this region. This is a typical problem of inverse methods when the geometry of the sampling network is sub-optimal and the source location is not surrounded by stations. This situation is similar to tomographic reconstructions, e.g., in medical applications, where the reconstruction quality is always best when measurements can be taken all around the phantom. Nonetheless, we conclude that the source location property of the LS-APC method provides reasonable results in all studied cases, even with the sub-optimal distribution of measurement stations.

We would like to point out that the Bayesian model selection allows to compare the likelihood of models for any set of matrices M_i , even if they are from different dispersion models and meteorological input data. The global maximum of the model likelihood for all cases is achieved with the Hysplit-GFS-0.5 configuration, see colorbars in Fig. 1.



5.2 Source term estimation

Source term estimates for the most likely locations for each dispersion model are given in Fig. 2. Full posterior densities are reported via their mean value (denoted by blue lines) and 99% highest posterior density regions (gray filled region). The source terms are accompanied by the computed total sum of activity with 99% uncertainty bounds in titles.

- 5 The officially reported total release activity was 342 GBq with a maximum release intensity of 108 GBq between October 12 and October 14 (Atomic Energy Agency, 2011b). In comparison with this value, the total activity was overestimated in the case of the Flexpart-GFS-0.5 simulation which estimated the total activity of the source term within interval [732, 1500] GBq (Fig. 2, left) while it is inside of the interval estimated by the Hysplit-GFS-0.5 simulation, [313, 667] GBq (Fig. 2, middle) as well as in the case of the Hysplit-GFS-1.0 simulation with estimated total activity within interval [331, 791] GBq (Fig. 2, right).
- 10 Moreover, one has to consider that these values are based on measurements of particulate iodine only. Thus, they are lower estimates for the total release which may also have included radioiodine gas. Given that and the fact that the best estimates from all models are higher than the reported release amount, it seems possible that the value reported in (Gitzinger et al., 2012) is too low. However, an alternative explanation for this may be that both atmospheric transport models produce a too short lifetime of particulate iodine. This, as for many other models, was found for Cs-137 attached to particles after the Fukushima
- 15 Dai-ichi accident (Kristiansen et al., 2016). The inversion would try to compensate a too strong loss of mass by increasing its emission.

With respect to the time variation of the release, all three estimated source terms have an emission activity peak during the reported maximum activity period around October 12 and October 14, confirming this aspect of the official report. The discrepancy in time scale of a few days is acceptable given that the sampling period for most measurements was 7 days. The

20 estimated release periods between mid-September and mid-November correspond well with the reported release period of September 8 to November 16 (Atomic Energy Agency, 2011b). The agreement is less good for the detailed time variation of the release since the emission peaks during this period occur not always at exactly the same time for Flexpart and Hysplit models. The results are accompanied by scatter plots between measured data y and reconstructed signal Mx in Fig. 3 for Flexpart-GFS-0.5 (left), Hysplit-GFS-0.5 (middle), and Hysplit-GFS-1.0 (right). Note that significantly lower marginal log-

25 likelihoods of the Flexpart-GFS-0.5 and Hysplit-GFS-1.0 models reported in Fig. 1 is due to only two measurements that are not explained well in the reconstruction. All other measurements are explained well.

5.3 Forward modeling of the iodine release

Using the estimated source location and source term, we can perform a forward run of the model and study the simulated consequences of the accidental release. For this purpose, we identify the most probable location of the release from all cases

30 according to our study (Fig. 1), which is the location with center at 19.75° E and 47.75° N obtained with the Hysplit-GFS-0.5 configuration with log-likelihood up to 340. Therefore, we perform a forward run with the Hysplit model and GFS input data with 0.5° resolution with the corresponding source term shown in the middle panel of Fig. 2. The forward model run was set up



in the same manner as the backward runs. The output concentrations presented in Fig. 4 are mean values in the layer between the surface and 100 meters above ground level.

The computed concentrations of I-131 are displayed in Fig. 4 for selected days, which are September 22 (left), October 22 (middle), and November 22 (right). The first two maps illustrate challenges for inverse modeling, since the aerosol was transported to areas where no measurement data are available. This also implies that the results may be very sensitive to the measurements from the station Budapest (denoted by the letter A in Fig. 4), which is the only station influenced in this case. This sensitivity will be studied in the next section.

The cumulated gamma dose for the whole 3-month period is displayed in Fig. 5 for the Hysplit-GFS-0.5 model with the same settings as in the case of concentrations. Results show that gamma dose amounts were largest in Hungary and Slovakia, while in the rest of Europe they were about two orders of magnitude smaller. However, Fig. 5 also shows that most of Europe was affected to some extent by the release. Notably, the simulation also shows that both the concentrations and dose amounts were very low even close to the release site. The maximum dose from the I-131 release during the studied 3-month period is approximately 0.001 mSv which is negligible, e.g., in comparison with the Czech natural radiation background of 3 mSv per year.

5.4 Sensitivity study

Since the distance between the measuring site in Budapest (denoted by the letter A in Fig. 1) and the IoI is only approximately 10 kilometers, the measured values at this station are often one order of magnitude higher than those from the other stations. Determining the source location could be thus dominated by those measurements. However, simulating the concentrations at such a short distance is inaccurate since the meteorological input data are much coarser than the distance from the source to the station, and also the SRS calculations are done on a coarser grid. Thus, the errors of the source-location sensitivity can be relatively large, which may influence the estimated source term.

To test the sensitivity of the results to the values from the Budapest station, we run the source location excluding those measurements. The results are given in Fig. 6. The data in this case are much less informative, hence the uncertainty in source location is much higher. Nevertheless, the maximum is always reached relatively close to the IoI facility. The maxima for individual dispersion models are 17.75° E 47.25° N for Flexpart-GFS-0.5, 18.75° E 48.25° N for Hysplit-GFS-0.5, and 19.25° E 46.75° N for Hysplit-GFS-1.0 while the exact location of the IoI is approximately 18.96° E 47.49° N. Thus, even in this poorly informative case, the location is identified with very good accuracy. In all three cases, the uncertainty increased significantly to the south of the IoI where no measured data are available.

Source term estimates for the most likely locations for each dispersion model are given in Fig. 7. Full posterior densities are reported via their mean value (denoted by blue lines) and 99% highest posterior density regions (gray filled region). The source terms are accompanied by the computed total sum of activity with 99% uncertainty bounds. Overall, the total activities of estimated Flexpart-GFS-0.5 and Hysplit-GFS-1.0 source terms are on the same level as in the previous case where measurements from Budapest are included while the Hysplit-GFS-0.5 result is reduced approximately four-times. Moreover, the release time profiles are different, with some peaks missing due to very low responses of these releases at the distant sensors.



Notice in particular that the period from 12-14 October with reported maximum releases is not captured anymore. This can be understood when considering Fig. 4. It can be seen that on the example days 22 September and 22 October, the whole released activity is transported south-east of the release site where no measurement stations are available except the Budapest station which is not used in this sensitivity study. This was the case also on many other days and explains why the LS-APC algorithm does not produce any releases in September and October in all Flexpart and Hysplit model runs when the Budapest station is excluded.

6 Conclusions

Low concentrations of iodine I-131 were detected in the atmosphere over Central Europe in the fall of 2011. After investigation, it was reported that I-131 was released from the Institute of Isotopes Ltd, Budapest, Hungary. In this study, the measurements of I-131 concentrations from several countries in Central Europe from fall 2011 were analyzed using two state-of-the-art dispersion models, Flexpart and Hysplit, and latest Bayesian techniques of source term estimation and source location. We used these techniques to retrieve both the source location as well as the magnitude and temporal variation of the release, assuming that neither the release location nor the source strength was known. The results correspond well with the true location of the source where all estimates are within 41 kilometers from the true location while the estimated total activity is higher than the reported released activity. Forward model simulations using the retrieved source term showed that large areas of Europe were affected by the release but air concentrations and total dosages of I-131 were well below regulatory limits everywhere and the situation did not pose a health risk.

The performance of the Bayesian methodology was also tested when using less informative data. For this, we removed the most informative measurements from the nearest measurement station. Even in this case, the algorithm was able to locate the source with high accuracy but with significantly higher uncertainty, and the source strength was particularly uncertain. The main reason for this large uncertainty was that all available measurement data (except for those taken at the one close-by station) were collected to the north of the release location. Therefore, releases could not be detected by this network during periods with northerly winds. This demonstrates the importance of the spatial distribution of measurement stations.

Acknowledgements. This research is supported by EEA/Norwegian Financial Mechanism under project MSMT-28477/2014 Source-Term Determination of Radionuclide Releases by Inverse Atmospheric Dispersion Modelling (STRADI). The authors would like to thank all the laboratories who provided monitoring data.

Appendix A: Truncated Gaussian distribution

Truncated normal distribution, denoted as $t\mathcal{N}$, of a scalar variable x on interval $[a; b]$ is defined as

$$t\mathcal{N}_x(\mu, \sigma, [a, b]) = \frac{\sqrt{2}\exp(-(x - \mu)^2)}{\sqrt{\pi}\sigma(\operatorname{erf}(\beta) - \operatorname{erf}(\alpha))}\chi_{[a, b]}(x), \quad (\text{A1})$$



where $\alpha = \frac{a-\mu}{\sqrt{2}\sigma}$, $\beta = \frac{b-\mu}{\sqrt{2}\sigma}$, function $\chi_{[a,b]}(x)$ is a characteristic function of interval $[a,b]$ defined as $\chi_{[a,b]}(x) = 1$ if $x \in [a,b]$ and $\chi_{[a,b]}(x) = 0$ otherwise. $\text{erf}()$ is the error function defined as $\text{erf}(t) = \frac{2}{\sqrt{\pi}} \int_0^t e^{-u^2} du$.

The moments of truncated normal distribution are

$$\langle x \rangle = \mu - \sqrt{\sigma} \frac{\sqrt{2}[\exp(-\beta^2) - \exp(-\alpha^2)]}{\sqrt{\pi}(\text{erf}(\beta) - \text{erf}(\alpha))}, \quad (\text{A2})$$

$$5 \quad \langle x^2 \rangle = \sigma + \mu \hat{x} - \sqrt{\sigma} \frac{\sqrt{2}[b \exp(-\beta^2) - a \exp(-\alpha^2)]}{\sqrt{\pi}(\text{erf}(\beta) - \text{erf}(\alpha))}. \quad (\text{A3})$$

For multivariate case, see (Tichý and Šmídl, 2016).



References

- A.J. Annunzio, G.S. Young, and S.E. Haupt. Utilizing state estimation to determine the source location for a contaminant. *Atmospheric environment*, 46:580–589, 2012.
- International Atomic Energy Agency. Low levels of iodine detected in Europe. *International Atomic Energy Agency (IAEA)*, 2011a.
- 5 International Atomic Energy Agency. Detection of I-131 in Europe. *International Atomic Energy Agency (IAEA)*, 2011b.
- A. Berchet, I. Pison, F. Chevallier, P. Bousquet, S. Conil, M. Geever, T. Laurila, J. Lavrič, M. Lopez, J. Moncrieff, et al. Towards better error statistics for atmospheric inversions of methane surface fluxes. *Atmospheric Chemistry and Physics*, 13(14):7115–7132, 2013.
- J.M. Bernardo and A.F.M. Smith. *Bayesian theory*, volume 405. John Wiley & Sons, 2009.
- C.M. Bishop. *Pattern recognition and machine learning*. springer, 2006.
- 10 M. Bocquet. Reconstruction of an atmospheric tracer source using the principle of maximum entropy. I: Theory. *Quarterly Journal of the Royal Meteorological Society*, 131(610):2191–2208, 2005.
- M. Bocquet. High-resolution reconstruction of a tracer dispersion event: application to ETEX. *Quarterly Journal of the Royal Meteorological Society*, 133(625):1013–1026, 2007.
- M. Bocquet. Inverse modelling of atmospheric tracers: Non-gaussian methods and second-order sensitivity analysis. *Nonlinear Processes in*
15 *Geophysics*, 15(1):127–143, 2008.
- J. Brandt, J.H. Christensen, and L.M. Frohn. Modelling transport and deposition of caesium and iodine from the Chernobyl accident using the DREAM model. *Atmospheric Chemistry and Physics*, 2(5):397–417, 2002.
- G. Cervone and P. Franzese. Monte Carlo source detection of atmospheric emissions and error functions analysis. *Computers & Geosciences*, 36(7):902–909, 2010.
- 20 X. Davoine and M. Bocquet. Inverse modelling-based reconstruction of the Chernobyl source term available for long-range transport. *Atmospheric Chemistry and Physics*, 7(6):1549–1564, 2007.
- L. Delle Monache, J.K. Lundquist, B. Kosovic, G. Johannesson, K.M. Dyer, R.D. Aines, F.K. Chow, R.D. Belles, W.G. Hanley, S.C. Larsen, et al. Bayesian inference and Markov chain monte carlo sampling to reconstruct a contaminant source on a continental scale. *Journal of Applied Meteorology and Climatology*, 47(10):2600–2613, 2008.
- 25 R.R. Draxler and G.D. Hess. Description of the HYSPLIT_4 modeling system. 1997.
- R.R. Draxler and G.D. Hess. An overview of the HYSPLIT_4 modelling system for trajectories. *Australian meteorological magazine*, 47(4):295–308, 1998.
- R.R. Draxler and G.D. Rolph. HYSPLIT (HYbrid Single-Particle Lagrangian Integrated Trajectory) model access via NOAA ARL READY website, 2003. URL <http://www.arl.noaa.gov/ready/hysplit4.html>. Accessed: 5.10.2016.
- 30 S. Eckhardt, A.J. Prata, P. Seibert, K. Stebel, and A. Stohl. Estimation of the vertical profile of sulfur dioxide injection into the atmosphere by a volcanic eruption using satellite column measurements and inverse transport modeling. *Atmospheric Chemistry and Physics*, 8(14):3881–3897, 2008.
- C. Forster, A. Stohl, and P. Seibert. Parameterization of convective transport in a Lagrangian particle dispersion model and its evaluation. *Journal of applied meteorology and climatology*, 46(4):403–422, 2007.
- 35 A.L. Ganesan, M. Rigby, A. Zammit-Mangion, A.J. Manning, R.G. Prinn, P.J. Fraser, C.M. Harth, K.-R. Kim, P.B. Krummel, S. Li, et al. Characterization of uncertainties in atmospheric trace gas inversions using hierarchical Bayesian methods. *Atmospheric Chemistry and Physics*, 14(8):3855–3864, 2014.



- C. Gitzinger, E. Henrich, and A. Ryan. Verification under the terms of article 35 of the EURATOM treaty, HU-12/01. 2012.
- S. Henne, D. Brunner, B. Oney, M. Leuenberger, W. Eugster, I. Bamberger, F. Meinhardt, M. Steinbacher, and L. Emmenegger. Validation of the Swiss methane emission inventory by atmospheric observations and inverse modelling. *Atmospheric Chemistry and Physics*, 16(6): 3683–3710, 2016.
- 5 M.B. Kalinowski, A. Becker, P.R.J. Saey, M.P. Tuma, and G. Wotawa. The complexity of CTBT verification. Taking noble gas monitoring as an example. *Complexity*, 14(1):89–99, 2008.
- A. Keats, E. Yee, and F. Lien. Bayesian inference for source determination with applications to a complex urban environment. *Atmospheric environment*, 41(3):465–479, 2007.
- I.V. Kovalets, S. Andronopoulos, A.G. Venetsanos, and J.G. Bartzis. Identification of strength and location of stationary point source of
10 atmospheric pollutant in urban conditions using computational fluid dynamics model. *Mathematics and Computers in Simulation*, 82(2): 244–257, 2011.
- N. I. Kristiansen, A. Stohl, D. J. L. Olivie, B. Croft, O. A. Søvde, H. Klein, T. Christoudias, D. Kunkel, S. J. Leadbetter, Y. H. Lee, K. Zhang, K. Tsigaridis, T. Bergman, N. Evangelidou, H. Wang, P.-L. Ma, R. C. Easter, P. J. Rasch, X. Liu, G. Pitari, G. Di Genova, S. Y. Zhao, Y. Balkanski, S. E. Bauer, G. S. Faluvegi, H. Kokkola, R. V. Martin, J. R. Pierce, M. Schulz, D. Shindell, H. Tost, and H. Zhang.
15 Evaluation of observed and modelled aerosol lifetimes using radioactive tracers of opportunity and an ensemble of 19 global models. *Atmospheric Chemistry and Physics*, 16(5):3525–3561, 2016.
- M. Krysta, M. Bocquet, and J. Brandt. Probing ETEX-II data set with inverse modelling. *Atmospheric Chemistry and Physics*, 8(14): 3963–3971, 2008.
- Ádám Leelőssy, Róbert Mészáros, Attila Kovács, István Lagzi, and Tibor Kovács. Numerical simulations of atmospheric dispersion of
20 iodine-131 by different models. *PloS one*, 12(2):e0172312, 2017.
- P. Liping, Z. Yu, Q. Hongquan, H. Tao, and W. Wei. Approach to identifying pollutant source and matching flow field. *Atmospheric Environment*, 73:1–10, 2013.
- J. Matthes, L. Groll, and H.B. Keller. Source localization by spatially distributed electronic noses for advection and diffusion. *IEEE Transactions on Signal Processing*, 53(5):1711–1719, 2005.
- 25 A.M. Michalak, A. Hirsch, L. Bruhwiler, K.R. Gurney, W. Peters, and P.P. Tans. Maximum likelihood estimation of covariance parameters for Bayesian atmospheric trace gas surface flux inversions. *Journal of Geophysical Research: Atmospheres*, 110(D24), 2005.
- Y. Morino, T. Ohara, and M. Nishizawa. Atmospheric behavior, deposition, and budget of radioactive materials from the Fukushima Daiichi nuclear power plant in March 2011. *Geophysical research letters*, 38(7), 2011.
- E. Nisbet and R. Weiss. Top-down versus bottom-up. *Science*, 328(5983):1241–1243, 2010.
- 30 B. Ristic, A. Gunatilaka, R. Gailis, and A. Skvortsov. Bayesian likelihood-free localisation of a biochemical source using multiple dispersion models. *Signal Processing*, 108:13–24, 2015.
- B. Ristic, A. Gunatilaka, and R. Gailis. Localisation of a source of hazardous substance dispersion using binary measurements. *Atmospheric Environment*, 142:114–119, 2016.
- A. Saiz-Lopez, J.M.C. Plane, A.R. Baker, L.J. Carpenter, R. von Glasow, J.C.G. Martín, G. McFiggans, and R.W. Saunders. Atmospheric chemistry of iodine. *Chemical Reviews*, 112(3):1773–1804, 2012.
- O. Saunier, A. Mathieu, D. Didier, M. Tombette, D. Quélo, V. Winiarek, and M. Bocquet. An inverse modeling method to assess the source term of the Fukushima nuclear power plant accident using gamma dose rate observations. *Atmospheric Chemistry and Physics*, 13(22): 11403–11421, 2013.



- P. Seibert. Inverse modelling of sulfur emissions in Europe based on trajectories. *Inverse Methods in Global Biogeochemical Cycles*, pages 147–154, 2000.
- P. Seibert and A. Frank. Source-receptor matrix calculation with a Lagrangian particle dispersion model in backward mode. *Atmospheric Chemistry and Physics*, 4(1):51–63, 2004.
- 5 I. Senocak, N.W. Hengartner, M.B. Short, and W.B. Daniel. Stochastic event reconstruction of atmospheric contaminant dispersion using Bayesian inference. *Atmospheric Environment*, 42(33):7718–7727, 2008.
- B. Simondi-Teisseire, N. Girault, F. Payot, and B. Clément. Iodine behaviour in the containment in Phébus FP tests. *Annals of Nuclear Energy*, 61:157–169, 2013.
- S.K. Singh and R. Rani. A least-squares inversion technique for identification of a point release: Application to fusion field trials 2007. *Atmospheric Environment*, 92:104–117, 2014.
- 10 V. Šmídl and A. Quinn. *The Variational Bayes Method in Signal Processing*. Springer, 2006.
- A.F. Stein, R.R. Draxler, G.D. Rolph, B.J.B. Stunder, M.D. Cohen, and F. Ngan. NOAA’s HYSPLIT atmospheric transport and dispersion modeling system. *Bulletin of the American Meteorological Society*, 96(12):2059–2077, 2015.
- A. Stohl, C. Forster, A. Frank, P. Seibert, and G. Wotawa. Technical note: The Lagrangian particle dispersion model FLEXPART version 6.2. *Atmospheric Chemistry and Physics*, 5(9):2461–2474, 2005.
- 15 A. Stohl, P. Seibert, G. Wotawa, D. Arnold, J.F. Burkhardt, S. Eckhardt, C. Tapia, A. Vargas, and T.J. Yasunari. Xenon-133 and caesium-137 releases into the atmosphere from the Fukushima Dai-ichi nuclear power plant: determination of the source term, atmospheric dispersion, and deposition. *Atmospheric Chemistry and Physics*, 12(5):2313–2343, 2012.
- M. Takeyasu and S. Sumiya. Estimation of dry deposition velocities of radionuclides released by the accident at the Fukushima Dai-ichi nuclear power plant. *Progress in Nuclear Science and Technology*, 4:64–67, 2014.
- 20 L.C. Thomson, B. Hirst, G. Gibson, S. Gillespie, P. Jonathan, K.D. Skeldon, and M.J. Padgett. An improved algorithm for locating a gas source using inverse methods. *Atmospheric Environment*, 41(6):1128–1134, 2007.
- O. Tichý and V. Šmídl. Non-parametric Bayesian models of response function in dynamic image sequences. *Computer Vision and Image Understanding*, 151:90–100, 2016.
- 25 O. Tichý, V. Šmídl, R. Hofman, and A. Stohl. LS-APC v1.0: a tuning-free method for the linear inverse problem and its application to source-term determination. *Geoscientific Model Development*, 9(11):4297–4311, 2016.
- M.E. Tipping and C.M. Bishop. Probabilistic principal component analysis. *Journal of the Royal Statistical Society: Series B (Statistical Methodology)*, 61(3):611–622, 1999.
- V. Winiarek, M. Bocquet, O. Saunier, and A. Mathieu. Estimation of errors in the inverse modeling of accidental release of atmospheric pollutant: Application to the reconstruction of the cesium-137 and iodine-131 source terms from the Fukushima Daiichi power plant. *Journal of Geophysical Research: Atmospheres*, 117(D5), 2012.
- 30 G. Wotawa, L.-E. De Geer, P. Denier, M. Kalinowski, H. Toivonen, R. D’Amours, F. Desiato, J.-P. Issartel, M. Langer, P. Seibert, et al. Atmospheric transport modelling in support of ctb verification—overview and basic concepts. *Atmospheric Environment*, 37(18):2529–2537, 2003.
- 35 X. Zheng and Z. Chen. Back-calculation of the strength and location of hazardous materials releases using the pattern search method. *Journal of hazardous materials*, 183(1):474–481, 2010.



Measuring site	Geographic coordinates	Number of measurements	Laboratory
Budapest	47°25'N, 19°20'E	12	NRIRR
Alt-Prerau	48°48'N, 16°28'E	1	AGES
Retz	48°45'N, 15°57'E	1	AGES
Usti nad Labem	50°40'N, 14°02'E	13	SUJB
Ostrava	49°50'N, 18°17'E	12	SURO
Ceske Budejovice	48°58'N, 14°28'E	14	SUJB
Praha	50°04'N, 14°27'E	16	SURO
Gdynia	54°31'N, 18°32'E	12	CLRP
Sanok	49°33'N, 22°12'E	12	CLRP
Katowice	50°16'N, 19°01'E	12	CLRP
Zielona Gora	51°56'N, 15°31'E	12	CLRP

Table 1. List of the sampling sites from which I-131 measurements were used in this study. NRIRR - *National Research Institute for Radiobiology and Radiohygiene* (regular on-site radiological measurements in NRIRR, http://www.osski.hu/info/ks/ksv_en.html), *Hungary*; AGES - *Austrian Agency for Health and Food Safety*, *Austria*; SUJB - *State Office for Nuclear Safety* (data retrieved from the Monitoring of Radiation situation database, MonRaS, http://www.sujb.cz/monras/aplikace/monras_en.html), *Czech Republic*; SURO - *National Radiation Protection Institute*, *Czech Republic*; CLRP - *Central Laboratory for Radiological Protection*, *Poland*.

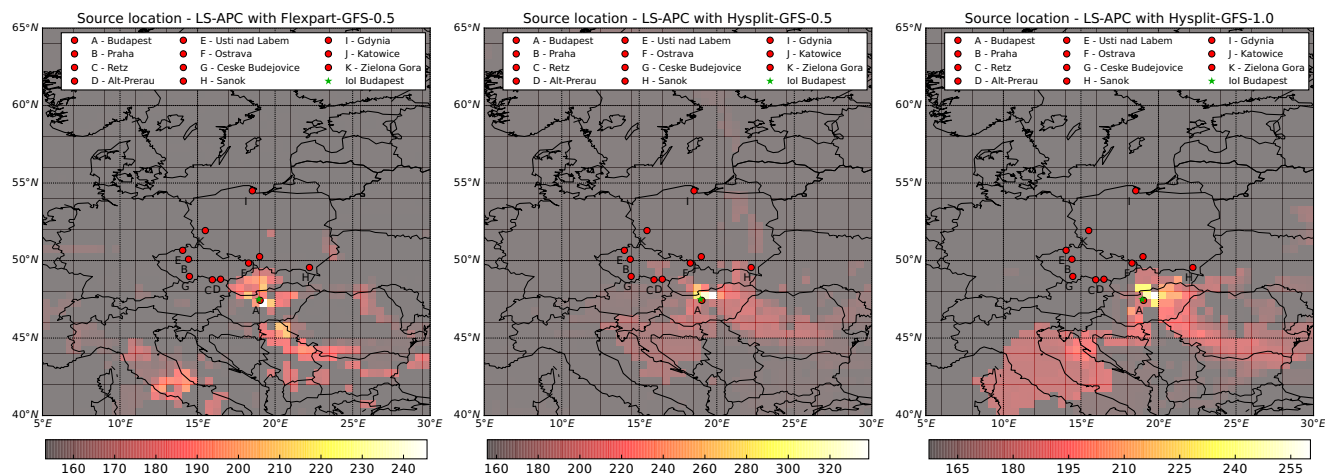


Figure 1. Source location via marginal log-likelihood where the observed data are explained by a release from a grid cell for all three tested combinations of dispersion model and meteorological data: Flexpart-GFS-0.5 (left), Hysplit-GFS-0.5 (middle), and Hysplit-GFS-1.0 (right). The measuring sites, Table 1, are displayed using red circles while the location of the Institute of Isotopes (IoI) Ltd. is displayed using a green star.

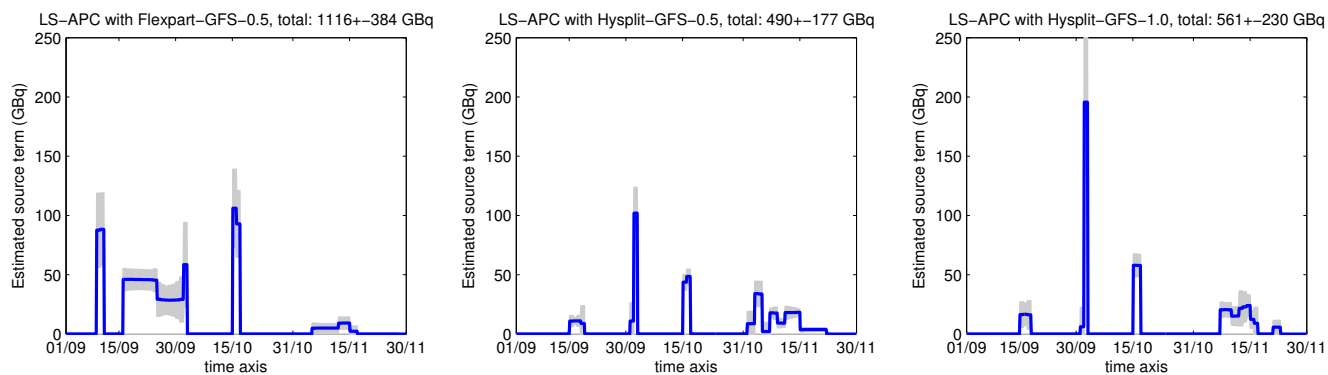


Figure 2. Estimated source terms at locations selected by the marginal likelihood method for all three tested combinations of dispersion models and meteorological data: Flexpart-GFS-0.5 (left), Hysplit-GFS-0.5 (middle), and Hysplit-GFS-1.0 (right). All locations correspond to the estimated release site, shown in Fig. 1.

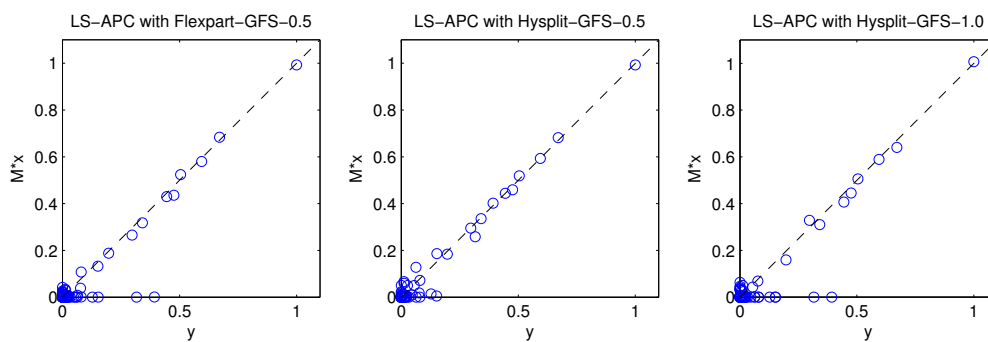


Figure 3. Scatter plots of the measurements y and the reconstructed signal Mx using the LS-APC algorithm with Flexpart-GFS-0.5 (left), Hysplit-GFS-0.5 (middle), and Hysplit-GFS-1.0 (right) forward model. The reconstructions are for the estimated source locations, shown in Fig. 1, and the mean values of the estimated source terms shown with blue lines in Fig. 2.

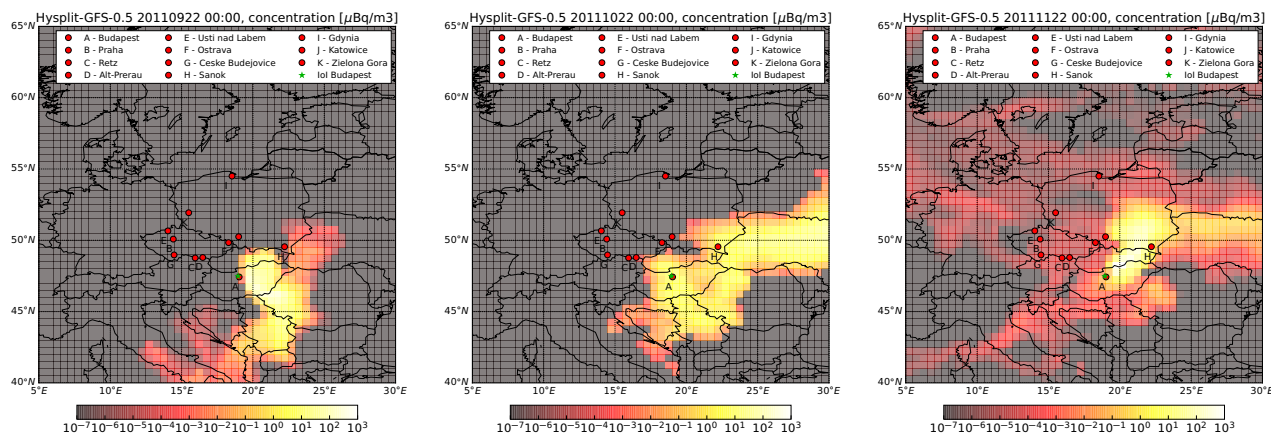


Figure 4. Maps of daily concentrations of I-131 for selected days (dates are reported at the top of each panel) using the Hysplit model with GFS input data with 0.5° resolution and with the source term given in Fig. 2, middle.

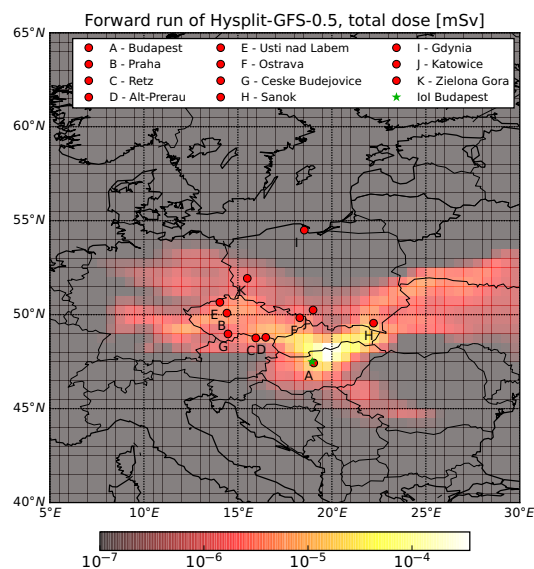


Figure 5. I-131 total dose for the whole 3-month study interval simulated using the Hysplit model with GFS input data with 0.5° resolution and with the source term given in Fig. 2, middle.

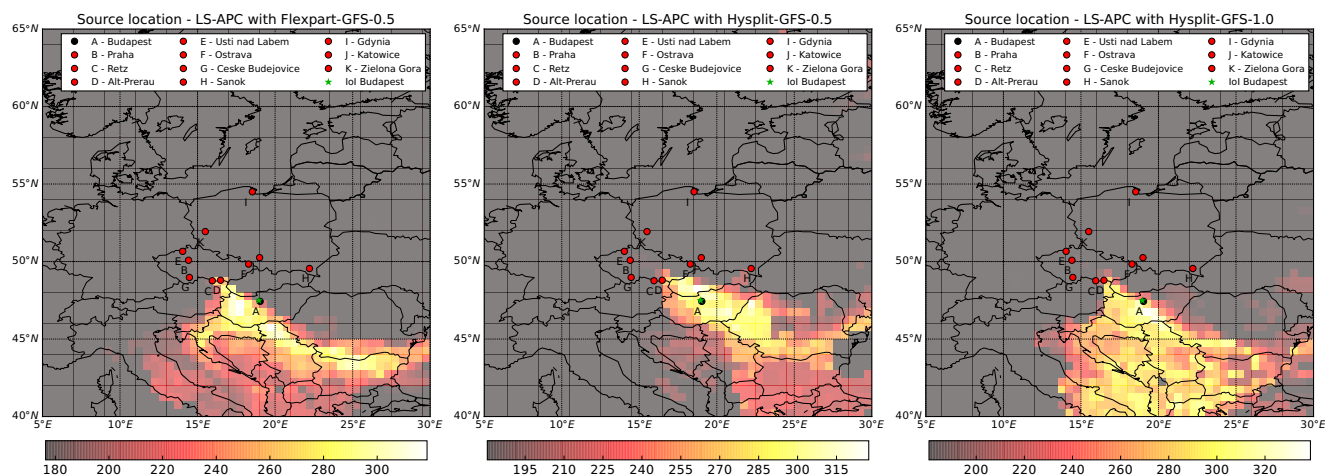


Figure 6. Sensitivity study of the source location using measurements without the Budapest station. Marginal log-likelihood that the observed data are explained by a release from a grid cell for each tested combination of dispersion model and meteorological data: Flexpart-GFS-0.5 (left), Hysplit-GFS-0.5 (middle), and Hysplit-GFS-1.0 (right). The measuring sites (see Table 1) are displayed using red circles while the location of the Institute of Isotopes (IoI) Ltd. is displayed using a green star and the excluded measuring station Budapest (denoted by A) is displayed using black circle.

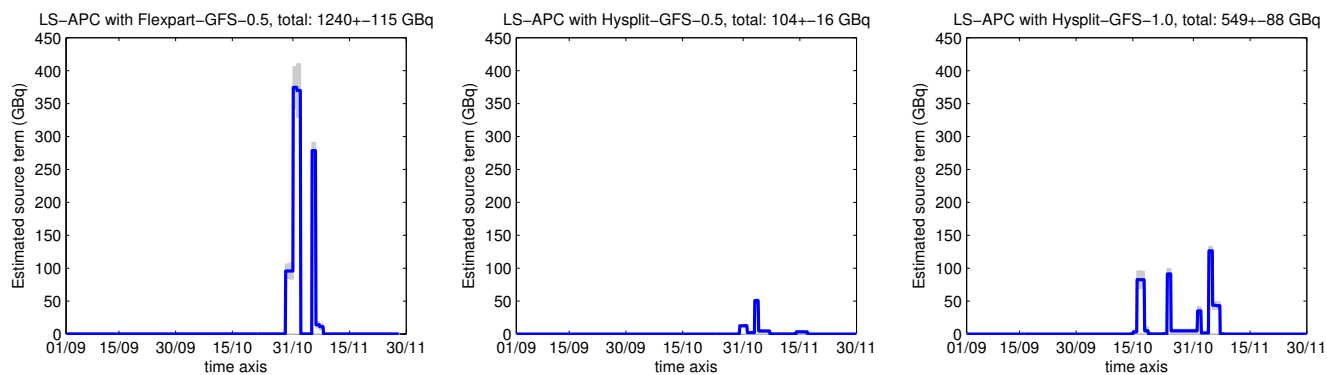


Figure 7. Estimated source terms at locations selected by the marginal likelihood method (Fig. 6) for all three tested dispersion models with excluded measurements from Budapest.